3.6

CONTROLLING THE EVOLUTION OF A SIMULATED HURRICANE THROUGH OPTIMAL PERTURBATIONS: INITIAL EXPERIMENTS USING A 4-D VARIATIONAL ANALYSIS SYSTEM

R. N. Hoffman*, C. Grassotti, J. M. Henderson, S. M. Leidner, G. Modica, and T. Nehrkorn
Atmospheric and Environmental Research, Inc.

1 INTRODUCTION

Theoretical and model studies have established that the dynamics governing the atmosphere can be extremely sensitive to small changes in initial conditions (e.g., Rabier et al. 1996). This suggests that the earth's atmosphere is chaotic. Chaos implies sensitivity to small perturbations. In a realistic numerical weather prediction (NWP) model, since small differences in initial conditions can grow exponentially, small but correctly chosen perturbations induce large changes in the evolution of the simulated weather. Current operational NWP practices—including data assimilation, generation of ensembles, and targeted observations—illustrate this daily (Hoffman 2002). A series of perturbations to the atmosphere might therefore be devised to effectively control the evolution of the atmosphere, if the atmosphere is observed and modeled sufficiently well. Hoffman (2002) hypothesized that as we observe and predict the atmosphere with more and more accuracy, we will become able to effect control of the atmosphere with smaller and smaller perturbations. The question addressed in the present study is how to calculate the optimal perturbations. Theory tells us that perturbations must have a special structure to grow explosively.

Hurricanes are a natural focus for weather control experiments. The motivation to control the weather is especially strong in the case of tropical cyclones. The AMS policy statement "Hurricane Research and Forecasting" (AMS 2000) summarizes the hazards of tropical cyclones over land: loss of life and nearly $5 billion (in 1998 dollars) annually in damage due to the storm surge, high winds and flooding. The economic cost continues to rise due to growing population and wealth in coastal regions. Further, hurricanes fit the profile of our hypothesis: hurricanes are difficult to predict. One reason is that hurricanes are very sensitive to specified initial conditions and boundary conditions, especially the sea surface temperature and topography. Warm sea surfaces provide latent and sensible energy for hurricanes to grow and rough land surfaces drain energy by frictional processes from hurricanes.

In our experiments we calculate perturbations to control simulations of Hurricanes Iniki and Andrew of 1992. We base our approach on a data assimilation method known as 4d-VAR which determines a small perturbation to the initial estimate of the atmosphere to optimally fit data over a 6 or 12 h window. See Hoffman et al. (2002) for a description of an early experiment that used 4d-VAR to change the position of Hurricane Iniki at the end of a six-hour interval. Our experiments are idealized both in terms of the simulation of the hurricanes and in terms of the method of control and should be considered prototypes. Our simulations of hurricanes could be improved with more sophisticated physical parameterizations and higher resolution. Further, we introduce perturbations to the model atmosphere as instantaneous changes. In a more realistic simulation the vector of control parameters that is optimized might be a description of the temporal and spatial patterns of feasible forcing. For example, these parameters might describe additional heating supplied to the atmosphere by a space solar power downlink in the 183 GHz water vapor spectral region. In spite of these simplifications, our experiments demonstrate the control of simulated hurricanes. The amount of energy required is very large, but we find that the perturbations amplitude decreases if we increase the resolution of the simulation system. Sensitivity experiments show in general that increasing degrees of freedom decrease the overall amplitude of the perturbation and that wind perturbations are more effective than others. In addition, downscaling experiments to higher resolution suggests that our results are relatively robust.

2 GENERATING PERTURBATIONS

A variety of possible means to generate perturbations was discussed by Hoffman (2002). In order to control a hurricane, one plausible approach is to use a space solar power (SSP) system to produce precise heating of the atmosphere. SSP has been proposed as a non-polluting inexhaustible source of energy. SSP would collect solar energy, and beam it down to earth. A downlink in microwave frequencies chosen so that the atmosphere

*Corresponding author: R. N. Hoffman, Atmospheric and Environmental Research, Inc., 131 Hartwell Avenue, Lexington, MA 02421. e-mail: rhoffman@aer.com

is transparent would minimize losses due to heating of the atmosphere. For weather control other frequencies would be chosen. Such an energy source could be modulated in time and directed at different locations. In the vertical, the energy deposition and hence heating is controlled by the transmission frequency and by the distribution of absorbing species, mainly water vapor and oxygen. Figure 1 illustrates this.

In Fig. 1 we plot heating rates as a function of altitude for different frequencies in the microwave spectrum for a top of the atmosphere power flux density of $1500\,\mathrm{Wm}^{-2}$. A single nominal-design SSP station might provide 6 GW of power which would cover an area 2×2 km at $1500\,\mathrm{Wm}^{-2}$. The heating rates are calculated for radiation vertically incident at the top of a standard tropical atmosphere. MonoRTM, a very accurate line-by-line radiative transfer model, is first used to calculate transmissivities ($\tau(z)$) every 0.5 km of altitude (z). These transmissivities increase monotonically from the top of the atmosphere to the surface and energy not transmitted through a layer is deposited in that layer. Thus heating rates may be calculated as

$$\frac{dT}{dt} = -\frac{F_0}{C_p \rho(z)} \frac{d\tau(z)}{dz}. \qquad (1)$$

Here T is temperature, t is time, F_0 is the flux at the top of the atmosphere, C_p is the specific heat of air, and ρ is the density of air. There are four major absorption bands in the microwave spectrum: the 22 GHz water vapor band, the 60 and 118 GHz oxygen bands, and the 183 GHz water vapor band. Figure 1a shows that while oxygen and water both absorb strongly, the absorption by the oxygen occurs mainly at levels in the atmosphere high above the bulk of the troposphere. The 183 GHz water vapor band presents the greatest opportunity to apply heating to the troposphere ($\sim 0-12$ km). Since water vapor in the atmosphere is very variable, the heating profiles will be a function of the meteorology, but this variation could be included in calculating the optimal orientation and power of the downlink. The 183 GHz band allows the vertical distribution of the heating to be controlled by tuning the transmission frequency in this part of the spectrum. This can be seen more clearly in Fig. 1b which shows heating rate profiles for selected frequencies near 183 GHz. As the frequency approaches 183 GHz the atmosphere becomes more opaque and more energy is absorbed at higher levels.

While SSP is a plausible system to control the atmosphere by heating, the prototype experiments reported here do not directly correspond to SSP. Instead, in our experiments we considered instantaneous changes to the atmospheric state. We explored allowing different variables to change, restricting the region where changes are allowed, and variations in the goal of the optimization. In some experiments we determine changes to the temperature structure of the atmosphere—closely related to but surely not the same as heating of the atmosphere. Our methods could be extended so that the control variables describe heating as a function of time and position instead of the atmospheric state. A further extension would use frequency and intensity of radiation at the top of the atmosphere as control variables. Ultimately a model of the SSP station would be added and the control variables for the optimization would be the actual control parameters determining the power, frequency, and orientation of the downlink.

3 The 4d-VAR METHOD

For weather forecasting, 4d-VAR finds the smallest perturbation at the start of each data assimilation period so that the solution best fits all the available data. 4d-VAR solves this complex nonlinear minimization problem iteratively, making use of the adjoint of a linearized version of the model. The operational use of 4d-VAR at the European Center for Medium Range Weather Forecasts and Météo France demonstrates the practical control of realistic simulations of the atmosphere. Current 4d-VAR practice finds the smallest global perturbation as measured by the *a priori*, or background, error covariances but it is possible to modify 4d-VAR to find the smallest perturbation measured in some other way. The MM5 implementation of 4d-VAR used in this study is described by Zou et al. (1997). It has been applied to assimilate zenith delay observations from global positioning system (GPS) satellites (De Pondeca and Zou 2001) and to assimilate cloud-cleared brightness temperatures from geostationary operational environmental satellite (GOES) sounders (Zou et al. 2001).

a. Initial perturbation cost function

The experiments reported here are based on variations of 4d-VAR. We consider the unperturbed simulation as reality. To mathematically define the objective function that will be minimized by 4d-VAR, we first define the unperturbed simulation U, from time 0 to T, with corresponding states $U(0)$ and $U(T)$. We then use 4d-VAR to find an optimal controlled simulation C by simultaneously minimizing the estimated damage and the difference from the initial state (i.e., $C(0)-U(0)$).

In these preliminary experiments, the size of the initial perturbation is measured in the cost function by a simple quadratic norm:

$$J(0) = \sum_{x,k} \frac{1}{S_{xk}^2} \left[\sum_{i,j} \{C_{xijk}(0) - U_{xijk}(0)\}^2 \right]. \qquad (2)$$

Here x defines the control vector variables (i.e., the temperature or the horizontal wind components or all variables), i, j, and k index the grid points in the three spatial dimensions. In Eq. (2), the flux or "coupled" form of the variables is used since this is the form of the primitive equations in the MM5. For example, $p_* u$ is the coupled eastward wind component, where p_* is the reference pressure difference between the bottom and top model boundaries. The reference state varies in the vertical only, therefore p_* depends only on the model surface topography.

The scales S_{xk} depends only on variable and layer. The scales are used to equalize the contributions of variables of different quantities and magnitudes. Effectively the scales are the relative costs of introducing perturbations at different levels or in different variables. In the present experiments S_{xk} is calculated as the maximum absolute difference between $U(0)$ and $U(\delta t)$ for each variable at each layer, with δt taken to be 40×60 s. In general these scales vary smoothly in the vertical, except that there is a maximum for eastward wind component in the upper troposphere in some cases. This discussion would have been simplified if we had simply specified the scales based on *a priori* arguments. Recall that the eventual control variables and cost function do not depend on the atmospheric state, but on the parameters describing the perturbations to the system.

b. *Damage cost function*

For the damage cost function experiments the total cost function is defined as

$$J_{\text{total}} = J(0) + \lambda \sum_t J_d(t). \tag{3}$$

Here the subscript d stands for damage and λ is a weighting factor. The damage cost function, J_d, is written in terms of physical damage estimates based on an empirical relationship between surface wind speeds and economic damage. The contribution to the cost function at each grid point is the product of the fractional wind damage (D_{ij}) and the property value (P_{ij}). Thus,

$$J_d(t) = \sum_{i,j} D_{ij}(t) P_{ij}. \tag{4}$$

The property values are unitless. The fractional damage (Unanwa et al. 2000) depends upon two threshold wind speeds; the lower threshold (U_0) is the wind speed at which damage to property first occurs, while the second (U_1) is the wind speed at which complete destruction occurs. Between these two threshold values, we model the increase in damage using a cosine curve

$$D(t) = \frac{1}{2}\left[1 + \cos\left(\pi \frac{U_1 - U(t)}{U_1 - U_0}\right)\right], \tag{5}$$

where $U(t)$ is the simulated horizontal wind speed. Note that U and hence D vary with location. In addition, the thresholds U_0 and U_1 might vary depending on property type at each grid point. In our basic experiments, Eq. (4) and Eq. (5) are evaluated only at time T (i.e., at the end of the 4d-VAR interval). In other experiments we evaluate D and J_d every 15 minutes for the last 2 h of the 4d-VAR interval and sum the contributions. In all cases $U_0 = 25\ \text{m s}^{-1}$ and $U_1 = 90\ \text{m s}^{-1}$. We experimented with the weighting factor λ; results presented here use $\lambda = 400\,000$.

c. *Control vector*

The control vector is a list of all the quantities that are allowed to be varied by the minimization. An example of an element of the control vector is the temperature at a particular grid point. In principle, one could minimize J with respect to the entire model state vector (that is, all prognostic variables at all grid points). For the MM5 these are the three-dimensional fields of $p_* u$, $p_* v$, $p_* T$, $p_* q$, p', and $p_* w$ (coupled eastward and northward wind components, temperature, and specific humidity, perturbation pressure, and coupled vertical velocity, respectively). In some versions of 4d-VAR all variables are allowed to vary even though only temperature, horizontal wind, and humidity observations are used. In such systems an additional constraint may be included in J to control the excitation of gravity waves. In other data assimilation systems p' and w, and perhaps q, are not allowed to vary. We experimented with several different control vectors.

4 EXPERIMENTAL PROCEDURES

We studied Hurricanes Iniki and Andrew of 1992 using the Penn State/NCAR Mesoscale Model 5 (MM5) 4d-VAR-system. MM5 produces very detailed and accurate simulations of tropical cyclones when high resolution and advanced physical parameterizations are used (e.g., Liu et al. 1999; Tenerelli and Chen 2001). However, in the current experiments, coarser, 20 km resolution is used for computational efficiency in most of the work reported here. For the purpose of our demonstration, the unperturbed MM5 simulation is taken to be reality.

a. *Hurricanes Iniki and Andrew*

Central Pacific Hurricane Iniki (1992) caused extensive damage to property and vegetation on parts of the Hawaiian Islands and killed six people (CPHC 1992; Lawrence and Rappaport 1994). The storm made landfall on Kauai at 0130 UTC 12 September 1992, with a central pressure of 945 hPa. Maximum sustained winds over land were

estimated at $60\,\mathrm{m\,s^{-1}}$ with gusts as high as $80\,\mathrm{m\,s^{-1}}$. For Iniki our experiments calculate optimal perturbations at 0600 UTC 11 September 1992.

Hurricane Andrew (1992) was extraordinary in several respects. Damage was in the tens of billions of dollars, a quarter of a million people were left homeless, and dozens of people died either directly or indirectly. Andrew made landfall in southern Florida near Homestead AFB at 0900 UTC 24 August with a central pressure of 922 hPa and surface winds gusting to $70\,\mathrm{m\,s^{-1}}$ (Wakimoto and Black 1994; Willoughby and Black 1996). Andrew crossed southern Florida in about 4 h. Our experiments for Andrew calculate optimal perturbations at 0000 UTC 24 August 1992. The hurricane's central pressure decreased very rapidly in the 48 h leading up to 0000 UTC 24 August 1992.

b. Mesoscale model

The MM5 used in our experiments is described by Grell et al. (1994) and by Dudhia (1993). In our experiments, the MM5 computational grid covers an approximately 4000×4000 km horizontal domain with ten "sigma" layers in the vertical from the surface to 50 hPa (or 100 hPa for the Andrew experiments). The tropical cyclones remain far enough from the domain edges that boundary effects are small during the course of the experiments. The sigma coordinate system is a terrain-following normalized pressure coordinate system (Holton 1992, section 10.3.1). The MM5 may be configured in many ways. However, only simple parameterizations of surface fluxes, radiative transfer, and cumulus convection are currently available in the MM5 4d-VAR system. Except as noted all experiments described here use nonhydrostatic dynamics, a 60 second time step and a 20 km polar stereographic grid. The physical parameterizations include the MRF PBL and the Anthes Kuo convection scheme. Large-scale stable (i.e., nonconvective) precipitation occurs whenever a layer reaches saturation. Excess moisture rains out immediately with no re-evaporation as it falls. Long wave radiation uses simple radiative cooling, with cloud effects included. The radiation computation occurs every 30 time steps.

c. Hurricane initialization in the gridded datasets

Gridded NCEP reanalysis fields (Kalnay et al. 1996) from the NCAR archives, and operational NCEP sea surface temperature (SST) analyses, were used to initialize the MM5 model and provide boundary conditions during the 4d-VAR and forecast periods. The boundary conditions define both the model state along the lateral boundaries and surface parameters such as SST, land use, and others. Other surface parameters were derived from the data bases included in the MM5 distribution. For Iniki the grid is 158×194, while for Andrew it is 200×200. Note that a smaller domain centered on the storm is plotted in all subsequent figures.

The available datasets have only a hint of an actual hurricane's strenth and structure. The use of high resolution satellite data to properly initialize a mesoscale model is an area of ongoing research. Consequently we add an analytic representation of a hurricane vortex using the method of Davis and Low-Nam (2001) 6 h before the start of our experiments (i.e., at $t = -6$) and let the model representation of the hurricane equilibrate during the 6 h leading up to the start of the 4d-VAR interval. The Davis and Low-Nam (2001) tropical cyclone bogussing system is part of the MM5 pre-processing procedures and was developed by NCAR and the Air Force Weather Agency (AFWA). Note that before the bogus storm is added the representation of the storm in the original data set is removed. The bogus storm is axisymmetric and is based on specifying the storm position and the radius and magnitude of the maximum wind in the lowest model layer. The maximum wind specified is supposed to represent the average wind speed at the radius of maximum wind speed and might be in the range of 75–90% of the best track wind speed. (The best track is the official description of a tropical cyclone based on all available information, collected either in real-time or later.) Given these parameters a Rankine wind vortex is used to generate the bogus lowest model level wind field. In a Rankine vortex the wind increases linearly with distance from the storm center to the radius of maximum wind and then decreases following a power law in distance. The exponent used here is $-3/4$. The bogus wind field at upper levels has the same Rankine vortex shape, but the wind speeds decrease according to a specified vertical profile. From the bogus wind field a temperature field is calculated to be in nonlinear, i.e., gradient, balance at all levels. Surface friction is ignored in this process, but the surface winds and other variables adjust within the first $1-2$ h.

The top row of panels of Fig. 2 shows the bogus storm for each case. The bogus storm was initiated 6 h earlier. Note in both cases that the bogus vortex is well defined, the wind speeds are high, and already possesses a clear wave number one asymmetry (in azimuth about the storm center). In this plot and in similar plots that follow, the wind speed is color coded according to the Saffir-Simpson scale and a single contour is plotted at $25\,\mathrm{m\,s^{-1}}$, the lowest wind speed that produces damage in our simulations. The Saffir-Simpson scale classifies tropical cyclones, including hurricanes, according to the maximum sustained wind: Up to 33 kt ($17.0\,\mathrm{m\,s^{-1}}$), they are called tropical depressions; up to 63 kt ($32.4\,\mathrm{m\,s^{-1}}$) tropical storms; up to 82 kt ($42.2\,\mathrm{m\,s^{-1}}$) Category 1 hurricanes; up to 95 kt ($48.9\,\mathrm{m\,s^{-1}}$) Category 2 hurricanes; up to 113 kt

(58.1 m s^{-1}) Category 3 hurricanes; and up to 135 kt (69.5 m s^{-1}) Category 4 hurricanes. These speed ranges correspond to the following colors in our wind speed plots: gray (TD), green (TS), yellow (Cat 1), red (Cat 2), blue (Cat 3), and purple (Cat 4).

Due to the relatively coarse resolution and simple parameterized physics used here, our simulations are only crude representations of observed track and intensity. The simulated storms are, in fact, still too weak, and, in the case of Iniki, too far to the west. For Iniki, we found it necessary to bogus the model vortex one degree to the east of the National Hurricane Center's best track position in order for the storm in the unperturbed simulations to track over Kauai as observed.

d. Generation of property values

Property values used in the computations are shown in the bottom panels of Fig. 2. Hurricane Iniki experiments use a basic two-dimensional property value field generated by smoothing topography. The smoother averages all points within 400 km resulting in a gradient of property values for nearshore water points that aids convergence of the minimizer. In the case of Hurricane Andrew this approach leads to a saddle point in the property value field over south Florida, with higher property values located farther north over Florida and over Cuba, which is not the desired result considering the actual value of property in south Florida. Therefore for Andrew we also used a refined property value field based on land use (Fig. 2). All urban grid points—which represent built-up cities with high property values—are initially assigned a relative value of 10000; all other grid points are temporarily assigned a value of zero. This initial property value field is then smoothed by averaging all points within 120 km. Land points that still have not been assigned a non-zero value are now set to a value of one. The end result is a property value field which strongly penalizes strong winds (> 25 m s^{-1}) in and near urban areas.

5 RESULTS

The experiment names given below refer to both the 4d-VAR analyses and the subsequent MM5 forecasts carried out beginning from the analyses. The forecast using unperturbed initial conditions is denoted U. Two experiments are reported in detail: an Iniki experiment using a property value cost function (Fig. 2a) based on topography denoted $C[T]$ and an Andrew experiment using a property value cost function based on land use denoted $L[T_a]$ (Fig. 2b). In the experiment names the "T" indicates that only temperature perturbations are permitted since temperature is the only variable in the control vector. Analogs to $C[T]$ with variations on the control vector are experiments $C[V]$, $C[w]$, $C[q]$, and $C[p']$—in which the control vector is composed of the horizontal wind components, the vertical velocity, the specific humidity, and the perturbation pressure, respectively. The maximum iterations allowed were 10 for the $C[\cdot]$ experiments and the $L[T_a]$ experiment. The minimization ended early for the $C[w]$ and $C[q]$ cases. In these, the minimizer could not determine a clearly-defined direction in which to proceed after five or six iterations.

a. Wind damage cost function baseline experiment

Figure 3 shows the cost function versus iteration for experiment $C[T]$. Note that the cost function asymptotes with increasing iterations, which indicates a smoothly-progressing minimization.

Figure 4 shows the structure of the perturbation δT at 950, 650, and 350 hPa for experiment $C[T]$. Note that the temperature scale is 4°C. In $C[T]$, a large cold temperature increment is present directly over the center of Iniki. These temperature increments are in direct opposition to the "warm core" thermodynamic structure of the hurricane and act to destroy the hurricane in place. At 950 hPa, the lowest model level, there is cooling close to the eye and heating to the west. At mid and upper levels there is a complex pattern of stronger heating and cooling. These patterns are not correlated between 650 hPa and 350 hPa. Patterns in the intervening layers show that these features twist and amplify with altitude. There is evidence of a banded structure away from the hurricane center that increases with altitude.

The ring of positive temperature increments from hours 2 through 8 (not shown but similar to the behavior shown in Fig. 8 for experiment $L[T_a]$) moves radially inward. Coincident with the collapse of the ring into a centrally located bubble of warm increments is a sudden and rapid decrease in sea-level pressure because sea-level pressure is proportional to the weight of the atmosphere above, which decreases as temperature increases. The increments temporarily disrupt the wind field at the appropriate time but there is a rapid increase in wind speed near the surface after 6 h. At 6 h the perturbations in temperature, vertical velocity and wind speed reach their greatest magnitude and are maximized close to the hurricane center. Thus, it appears that in experiment $C[T]$ that the kinetic wind energy is temporarily converted into thermal (potential) energy. At the same time that the perturbations focus on the hurricane center, other wave-like perturbations propagate radially outward at greater distances from the storm center. The effect of these changes on the full wind fields (Fig. 5) is to effectively suppress the winds to near or below the critical damaging wind level of 25 m s^{-1} at 6 h, and at 6 h only. It should be

noted that the extent and intensity of the winds increased rapidly in the hours following this time in the $C[T]$ experiments. However, this experiment was extremely successful at limiting the number of grid points with damaging winds at 6 h. We note that the sea-level pressure field (which is related to the overall temperature through the depth of the atmosphere) appeared to be temporarily mispositioned with respect to the wind field close to the time of the wind damage cost function evaluation.

b. Parameter sensitivity experiments

We conducted additional sensitivity experiments in which the control vector is restricted to each of V, w, q, and p' in turn. It should be noted that the scales (S_{xk} of Eq. (2)) used affect the numeric results, but perturbations calculated in experiments described here in which a single variable is the control vector are less influenced by the scales. Figure 6 shows the perturbations for these parameter sensitivity experiments. The largest perturbations in each case are near the center of Iniki. Increments of smaller magnitude typically have a concentric pattern of alternating sign at larger distance from the storm's center. That the larger increments occur at the center of the storm is expected, since hurricanes are largely sustained by physical processes in the storm's eyewall. The concentric patterns appear wave-like, propagating both inward and outward with respect to the hurricane center.

The position of Iniki in the surface wind fields at 6 h (not shown) is, in general, farther north and west than in the unperturbed simulation. The extent of damaging winds is substantially reduced in $C[V]$, though less so in $C[w]$. In experiment $C[p']$, it is noteworthy that gravity waves advance from the lateral boundaries at $70\ \mathrm{m\ s^{-1}}$ and interact with the inner environment of the storm at 6 h. Apparently this is the most efficient way for 4d-VAR to weaken the storm under the constraints of experiment $C[p']$. Strong horizontal wind increments near the center of the storm in $C[V]$ are similar in size and form to what was found in experiments where all variables are allowed to vary. This is consistent with the fact that 4d-VAR reduces wind damage most efficiently via changes in the initial horizontal wind field. In experiment $C[q]$ we note that there are isolated regions of supersaturation (relative humidity greater than 100%) that are a consequence of large positive perturbations close to the center of the storm and over the large island of Hawaii. These strongly supersaturated regions only occur early in the $C[q]$ simulation.

c. Refined property damage cost function

Our first Andrew experiment using topography-based property values (not reported here) suggested several refinements, including a refined cost function, that were then implemented for experiment $L[T_a]$. For our current Hurricane Andrew experiment $L[T_a]$ we used land use to define the property values and summed Eq. (4) every fifteen minutes over hours four through six of the 4d-VAR interval. Examination of the $L[T_a]$ simulation at five minute intervals shows that the storm's intensity is decreased throughout the time interval 4 to 6 h, however, strong surface winds regenerate after 6 h. Figure 7 shows the structure of the perturbation δT at 950, 650, and 350 hPa for experiment $L[T_a]$. The perturbations are qualitatively similar to the perturbations of other experiments we conducted with concentric banded patterns at large distance from the hurricane center. In this particular case the larger magnitude small scale structures are most apparent at 650 hPa. The time evolution (Fig. 8) of the temperature perturbations for experiment $L[T_a]$ is similar to those for the other Andrew cases we have studied, though features in the δT field near the hurricane center are of even smaller scale. The reduction of surface wind speeds appears as the extensive region of reduced 950 hPa wind speeds over and near the southeast Florida coastline at hour 6. The slight repositioning of the storm by 4d-VAR may also contribute to the few very large wind increment vectors at this time. Figure 9 shows the evolution of the surface wind field for the unperturbed simulation U_a and for experiment $L[T_a]$. As Andrew advances on the Florida coastline from 4 to 6 h in this experiment, the $25\ \mathrm{m\ s^{-1}}$ damaging wind contour folds in on the west side of Andrew to satisfy our requirement to minimize wind damage until 6 h. By 8 h this contour has resumed a more circular shape as damaging winds spread inland.

d. Robustness of the solution

The Andrew 4d-VAR solution for $L[T_a]$ and the $t = 0$ U_a state were also used to initialize high resolution enhanced physics simulations. These runs retain the 10 layer vertical structure, but use a grid that is three times finer in both horizontal directions, i.e., with a resolution of ~ 6.67 km, and a time step of 20 seconds. For convenience we will refer to this as the 7 km grid. The high resolution 7 km model simulations use enhanced physics including the advanced Schulz explicit moisture microphysics, the more sophisticated Kain-Fritsch cumulus convection parameterization, the CCM2 radiative shortwave heating and longwave cooling and a multilayer soil model.

The general characteristics of the pairs of simulated surface wind fields match fairly well. This means that the perturbations calculated at 20 km are still effective at 7 km. The experiments described so far are what may be called perfect model experiments in that 4d-VAR and our simulations use exactly the same model of the atmo-

sphere. The 7 km experiments show to what extent a perturbation calculated using one approximation to the atmosphere works in a situation with more realistic dynamics. Thus comparing the result of transplanting the 20 km perturbations into a 7 km simulation is a test of the robustness of our methodology.

In summary, all wind damage-based cost function experiments share some features:

1. experiments that permit perturbations to the temperature and/or wind fields are successful both numerically and meteorologically in reaching the goal of minimizing surface wind speeds.

2. the controlled hurricane is noticeably weakened but only repositioned slightly by 4d-VAR. In the two cases presented here, the steering flow is robust and so 4d-VAR likely finds weakening the storm easier than repositioning.

3. weakening largely is accomplished by cooling mid-levels of the storm, though the full mechanism is not fully understandable based on our limited number of cases.

4. the effect of instantaneous initial perturbations is transient, suggesting the need for repeated "applications" of the control mechanism.

This commonality suggests that these experiments describe robust responses to the meteorological and numerical questions that have been posed. We have strived to lay the ground work for more comprehensive treatment of the problem.

6 THE FUTURE

The preliminary study described here shows that 4d-VAR can be used to calculate "optimal" perturbations to control the intensity of a simulated tropical cyclone. Clearly it will be a long time before it is possible to control a tropical cyclone in reality. While the results reported here are preliminary in many aspects, they point the way towards further work. A necessary prerequisite is the ability to forecast tropical cyclones accurately. Beyond this, advances in several technical areas are needed. These are discussed in the following paragraphs.

In addition, a number of problems must be solved in the political, economic, and legal realms. For inhabitants of New Orleans, eliminating a hurricane threat to that city may take precedence over all else, yet farmers in the Mid-West might suffer without the resulting rain. This example shows that many competing factors must be considered in defining the cost function to be optimized. These "side issues" may prove more difficult to overcome than the science and engineering issues.

Items 1, 2, and 3 below relating to the calculation of the perturbations could be usefully examined now with computer simulations that would naturally follow on this study. Advances in items 4 and 5—improved models and observations of the atmosphere—will occur naturally as we improve NWP. Item 6, the creation of perturbations will require engineering new systems. The last two items—improved observations and the creation of perturbations—may require new space-based assets.

1. **Calculation of realistic perturbations.** Solving for the optimal perturbation using a more realistic model is difficult due to the number of degrees of freedom required to represent the atmosphere adequately and the nonlinear and sometimes discontinuous nature of the physics governing the atmosphere. With higher resolution and more degrees of freedom, effective perturbations are expected to require smaller magnitudes but more detailed structure. Incremental 4d-VAR (Lorenc 1997; Rabier et al. 2000), will allow the most sophisticated physics to be used for the trajectory calculation, but simpler physics for the 4d-VAR calculation. The incremental approach eliminates the need to use full resolution in the linear models, and the use of limited physics eliminates the need to code the adjoint of the most complex packages. These changes can increase the speed of the gradient calculation.

2. **Calculation of feasible perturbations.** The 4d-VAR methodology could be extended for this purpose. A control vector could be developed first in terms of heating perturbations continuous in time over a three- or six-hour period, later in terms of the radiation perturbations at the top of the atmosphere, and finally in terms of the orientation, power, and frequency of the space solar power downlink antenna.

3. **Overcoming chaos.** The control must be effected at significant time lags to minimize the size of the perturbations, yet the system is inherently unpredictable at long lead times. In general, theoretical predictability studies (Lorenz 1969) suggest that doubling the resolution of the observations will only increase predictability by an amount similar in magnitude to the timescale of the motions of the smallest resolved phenomena. For example, since the timescale for the evolution of a thunderstorm is smaller than one hour, observing details of individual thunderstorms will improve predictability by no more than one hour. Therefore controlling small-scale phenomena may be difficult.

One approach is to continuously monitor and control the system by adding perturbations regularly. Another approach is to control the environment of the phenomena of interest. This viewpoint has some validity for the case of hurricanes. Internal hurricane dynamics have a time scale of a day or less. This limits how far back in time we can go to calculate optimal perturbations. But hurricane tracks are greatly affected (one could say "steered") by the large scale upper level winds and hurricanes cannot maintain intensity and structure in the presence of environmental vertical wind shear. So, an alternative is to control the large scale wind field several days or even a week in advance to affect the hurricane's path or intensity, or to prevent a hurricane from forming.

4. **Improved NWP.** Projecting future computer and space technology trends is difficult. However, the technical roadmap for improving NWP and data assimilation is well established, and the timing of future progress has been estimated (e.g. ECMWF 1999).

5. **Improved atmospheric observations.** Satellites provide a large volume of information, but not always in the right place, or of the right variable, or sufficiently accurate. New instruments on the Terra, Aqua, and Aura satellites hold the promise to fill some of these gaps. Future space-based lidar sensors should be valuable by providing more direct and very accurate measurements of atmospheric properties including winds.

6. **Creation of perturbations.** Optimal perturbations, while small in amplitude, may be large in scale and require substantial amounts of energy. The costs of controlling a hurricane in our simulation experiments in terms of energy required are enormous. In preliminary experiments we did find that halving the grid size more than halved the energy required. If this trend continues down to sub-kilometer-scales (scales that we would like to use for more accurate forecasting in any case), then control of large-scale weather in the future becomes much more believable.

With regard to demonstrating effective control of weather, we first note that in spite of our desire for perfection, observations and predictions are always somewhat uncertain. Modern data assimilation uses estimation theory to treat NWP, whether on the global scale or some smaller scale, in a probabilistic sense. We can keep track of uncertainty with Kalman filters or ensemble methods so that we can tell if the predicted impact of some treatment is small or large compared to the predicted uncertainty. Then, if we also simulate the effect of the perturbation, we can perform significance testing before the weather control activity begins!

Our approach of using accurate calculations of the sensitivity of the atmosphere to determine precise perturbations might also be applied to smaller scales as a demonstration test. With current observation systems, it may be possible to take this approach with cloud scale models in the next several years. Real time applications may be far off since the time scales associated with cloud scales are so small compared to current computation resources. However, for the purpose of weather modification experimentation, one could make a probabilistic forecast, say, for untreated cases and validate these probabilistic forecasts with observations. Then having the capability to make validated probabilistic cloud scale forecasts, it becomes possible to state the significance of the difference between an observed treated result and the corresponding forecast untreated result. Furthermore, if one models the effect of the treatment, then one could also compare a forecast treated case and the untreated observation.

This probabilistic approach could be applied now for simple stratiform rain situations. An optimistic assessment is that it will likely be 5 and perhaps 10 years before the current state of the art for observing and simulating cumulus clouds has advanced enough that the uncertainty of the probabilistic forecast is sufficiently small so that useful conclusions may be drawn. In the time range of 10-20 years, our ability to forecast hurricanes may have advanced so much that we will have sufficient confidence to begin control experiments using aircraft contrails or aircraft-dispersed surface oils. If successful, such experiments may provide additional impetus to speed the development of space solar power. Active control of the large-scale weather patterns to reduce the severity of droughts, to decrease the number of severe tornadoes, and to reduce damage due to hurricanes, may then become a reality 40-50 years from now.

Acknowledgement This work was supported by the NASA Institute for Advanced Concepts (NIAC) through a grant from the Universities Space Research Association (USRA).

References

AMS, 2000: Hurricane research and forecasting. *Bull. Am. Meteorol. Soc.*, **81**, 1341–1346.

CPHC, 1992: Tropical cyclones report for the central Pacific. Technical Memorandum NWS-PR-38, Central Pacific Hurricane Center, NOAA, Washington, DC, [http://205.156.54.206/pr/hnl/cphc/pages/hurrclimate.html].

Davis, C. and S. Low-Nam, 2001: The NCAR-AFWA tropical cyclone bogussing scheme. Technical Memorandum, Air Force Weather Agency (AFWA), Omaha, NE, [http://www.mmm.ucar.edu/mm5/mm5v3/tc-report.pdf].

De Pondeca, M. F. V. and X. Zou, 2001: A case study of the variational assimilation of GPS zenith delay observations into a mesoscale model. *J. Applied Meteorol.*, **40**, 1559–1576.

Dudhia, J., 1993: A nonhydrostatic version of the Penn State-NCAR mesoscale model: Validation tests and simulation of an Atlantic cyclone and cold front. *Mon. Weather Rev.*, **121**, 1493–1513.

ECMWF, 1999: A strategy for ECMWF, 1999-2008. Miscellanenous publication, Eur. Cent. for Med. Range Weather Forecasts, Reading, England, 16 pp.

Grell, G. A., J. Dudhia, and D. R. Stauffer, 1994: A description of the fifth-generation Penn State/NCAR mesoscale model (MM5). Technical Note 398+1A, NCAR, 122 pp.

Hoffman, R. N., 2002: Controlling the global weather. *Bull. Am. Meteorol. Soc.*, **83**, 241–248.

Hoffman, R. N., J. M. Henderson, and S. M. Leidner, 2002: Using 4d-VAR to move a simulated hurricane in a mesoscale model. *19th Conference on weather Analysis and Forecasting/15th Conference on Numerical Weather Prediction*, American Meteorological Society, Boston, MA, San Antonio, Texas, J137–J140, paper JP4.4.

Holton, J. R., 1992: *An Introduction to Dynamic Meteorology*. Academic, New York, third edition, 511 pp.

Kalnay, E., M. Kanamitsu, R. Kistler, W. Collins, D. Deaven, L. Gandin, M. Iredell, S. Saha, G. White, J. Woollen, Y. Zhu, A. Leetmaa, B. Reynolds, M. Chelliah, W. Ebisuzaki, W. Higgins, J. Janowiak, K. C. Mo, C. Ropelewski, J. Wang, R. Jenne, and D. Joseph, 1996: The NCEP/NCAR 40-year reanalysis project. *Bull. Am. Meteorol. Soc.*, **77**, 437–471.

Lawrence, M. B. and E. N. Rappaport, 1994: Eastern North Pacific hurricane season of 1992. *Mon. Weather Rev.*, **122**, 549–558.

Liu, Y., D.-L. Zhang, and M. K. Yau, 1999: A multiscale numerical study of Hurricane Andrew (1992). Part II: Kinematics and inner-core structures. *Mon. Weather Rev.*, **127**, 2597–2616.

Lorenc, A. C., 1997: Development of an operational variational assimilation scheme. *J. Meteorol. Soc. Japan*, **75**, 339–346.

Lorenz, E. N., 1969: The predictability of a flow which possesses many scales of motion. *Tellus*, **21**, 289–307.

Rabier, F., H. Järvinen, E. Klinker, J.-F. Mahfouf, and A. Simmons, 2000: The ECMWF operational implementation of four-dimensional variational assimilation. I: Experimental results with simplified physics. *Q. J. R. Meteorol. Soc.*, **126**, 1143–1170.

Rabier, F., E. Klinker, P. Courtier, and A. Hollingsworth, 1996: Sensitivity of forecast errors to initial conditions. *Q. J. R. Meteorol. Soc.*, **122**, 121–150.

Tenerelli, J. E. and S. S. Chen, 2001: High-resolution simulations of Hurricane Floyd using MM5 with vortex-following mesh refinement. *14th Conference on Numerical Weather Prediction*, American Meteorological Society, Boston, MA, Fort Lauderdale, Florida, J52–J54.

Unanwa, C. O., J. R. McDonald, K. C. Mehta, and D. A. Smith, 2000: The development of wind damage bands for building. *Journal of Wind Engineering and Industrial Aerodynamics*, **84**, 119–149.

Wakimoto, R. M. and P. G. Black, 1994: Damage survey of hurricane Andrew and its relationship to the eyewall. *Bull. Am. Meteorol. Soc.*, **75**, 189–200.

Willoughby, H. E. and P. G. Black, 1996: Hurricane Andrew in Florida: Dynamics of a disaster. *Bull. Am. Meteorol. Soc.*, **77**, 543–549.

Zou, X., F. Vandenberghe, M. Pondeca, and Y.-H. Kuo, 1997: Introduction to adjoint techniques and the MM5 adjoint modeling system. Technical Note 435-STR, NCAR, Boulder, CO.

Zou, X., Q. Xiao, A. E. Lipton, and G. D. Modica, 2001: A numerical study of the effect of GOES sounder cloud-cleared brightness temperatures on the prediction of Hurricane Felix. *J. Applied Meteorol.*, **40**, 34–55.

Fig. 1: Heating rates (degrees/hour) as a function of frequency (GHz) and height (km). Calculations are for the standard tropical atmosphere assuming vertically incident radiation with power flux density of 1500 Wm^{-2}. The whole microwave spectrum and heights to 25 km are shown in (a). Values greater than 3 $^{\circ}$ h^{-1} are reset to that value for plotting. This affects higher levels in the oxygen bands where absorption is strong and density is low. Selected profiles near the 183 GHz water vapor resonance are plotted in (b). Here as height increases, density decreases, so that peak heating rates are larger for more opaque frequencies.

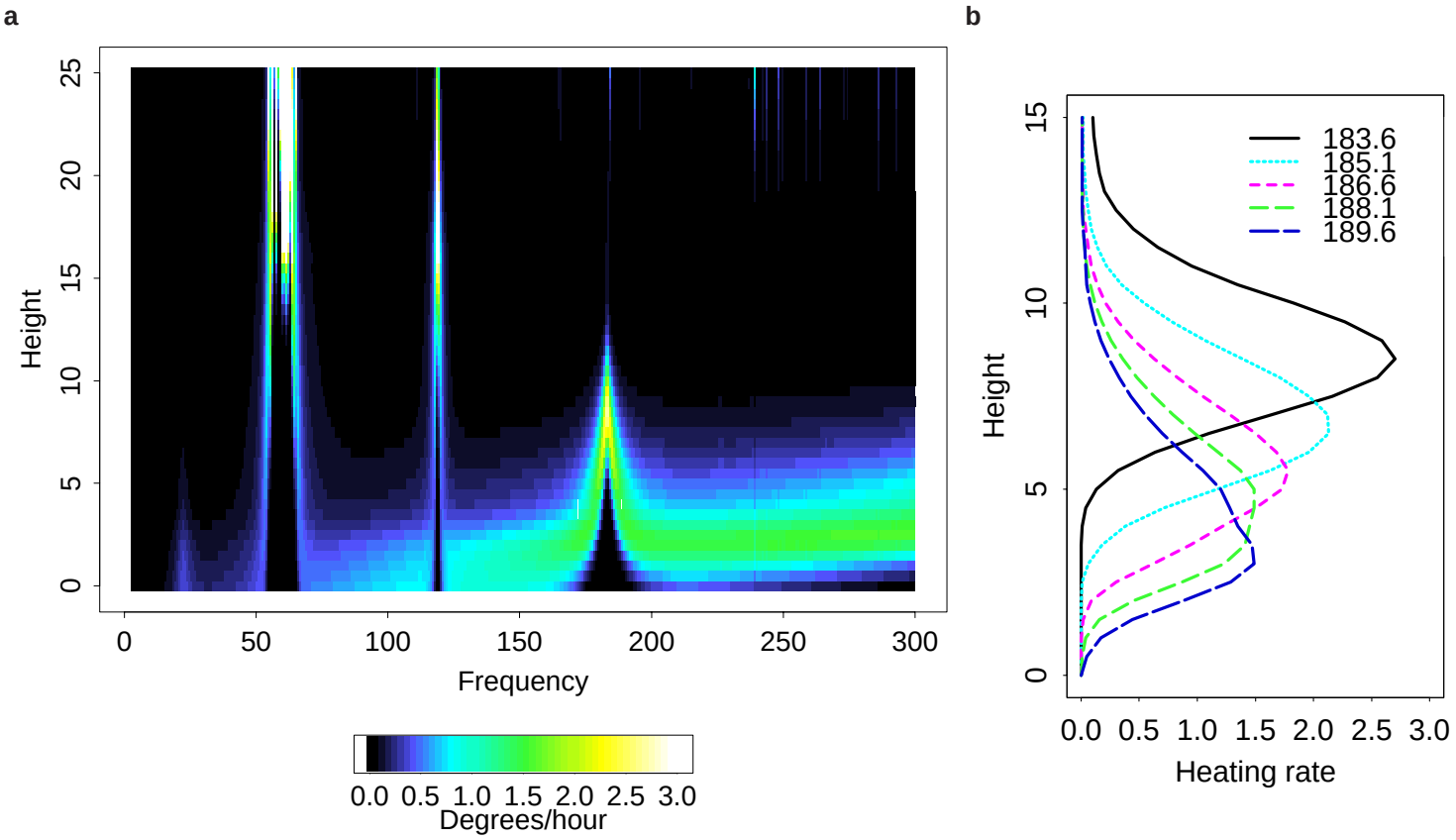

Fig. 2: Initial conditions and property values used in the experiments for Iniki and Andrew. Initial conditions show surface pressure and winds at the start of the 4d-VAR interval for Iniki and Andrew as depicted by the bogus procedure. Surface pressure is contoured in hPa, wind speed in $m\,s^{-1}$ is color coded, and wind barbs are in kts. Wind speed is color coded according to the Saffir-Simpson scale and the damaging wind contour $25\,m\,s^{-1}$ is plotted. Iniki property values are based on smoothed topography and Andrew property values are based on land use. See text for details. Property values are unitless, but might be considered tens of thousands of dollars per square kilometer.

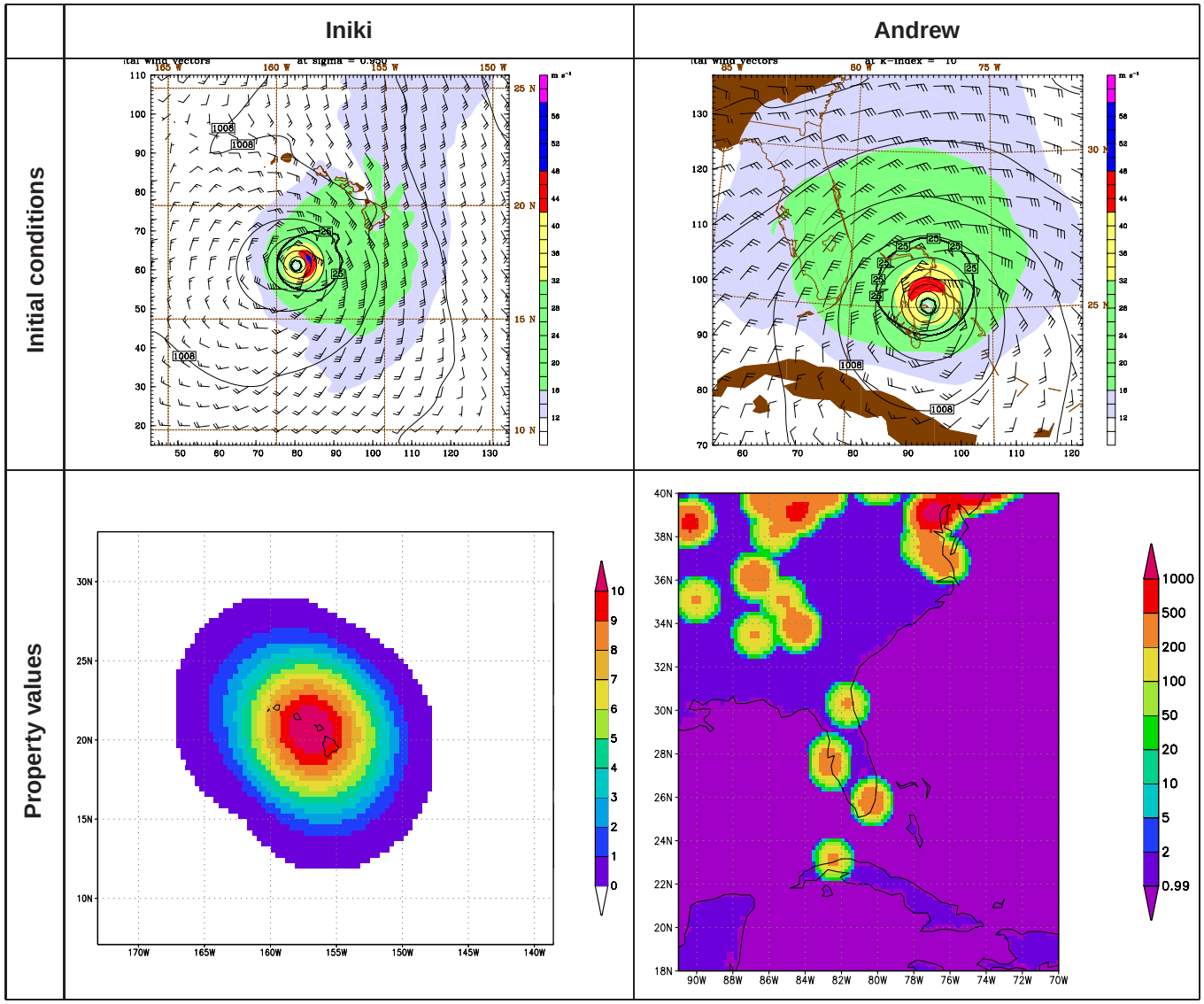

Fig. 3: Cost function versus iteration for experiment $C[T]$. The total cost function (in thousands) and the individual parts of the cost function at $t = 0$ and 6 h are shown as solid, dotted, and dashed lines, respectively.

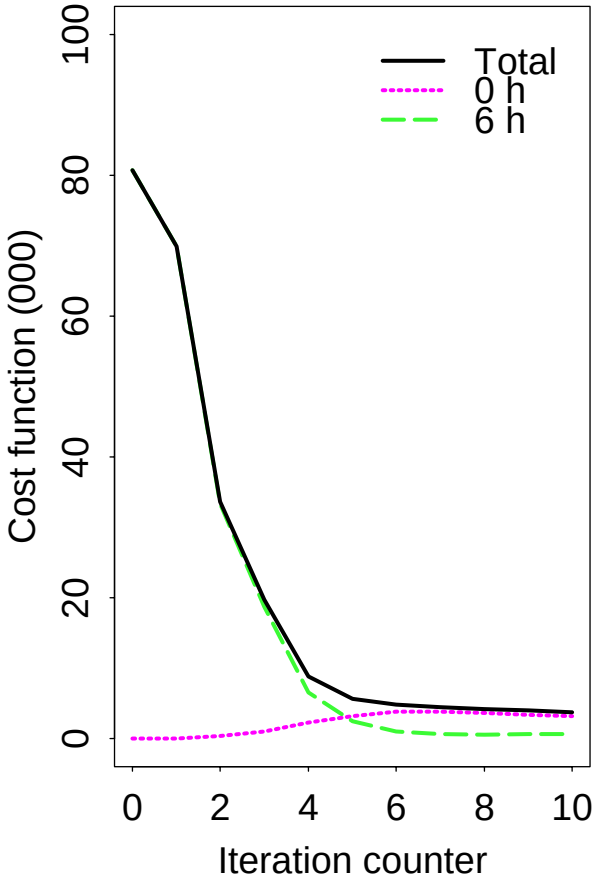

Fig. 4: Structure of the initial perturbation for experiment $C[T]$. Horizontal slices of δT are shown at 950, 650, and 350 hPa. Temperature in degrees C is color coded.

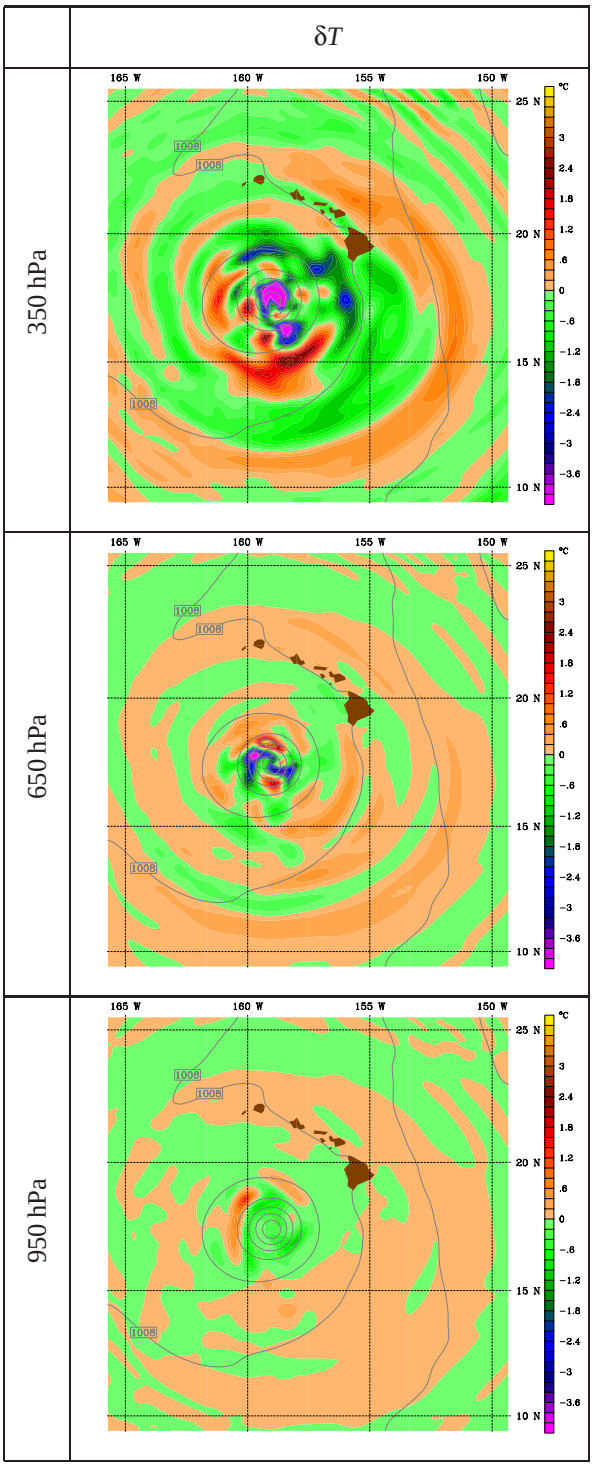

Fig. 5: Evolution of the surface wind field for the unperturbed simulation U and for experiment $C[T]$. Wind speed is color coded according to the Saffir-Simpson scale and the damaging wind contour $25\,\mathrm{m\,s^{-1}}$ is plotted at 4, 6, and 8 h.

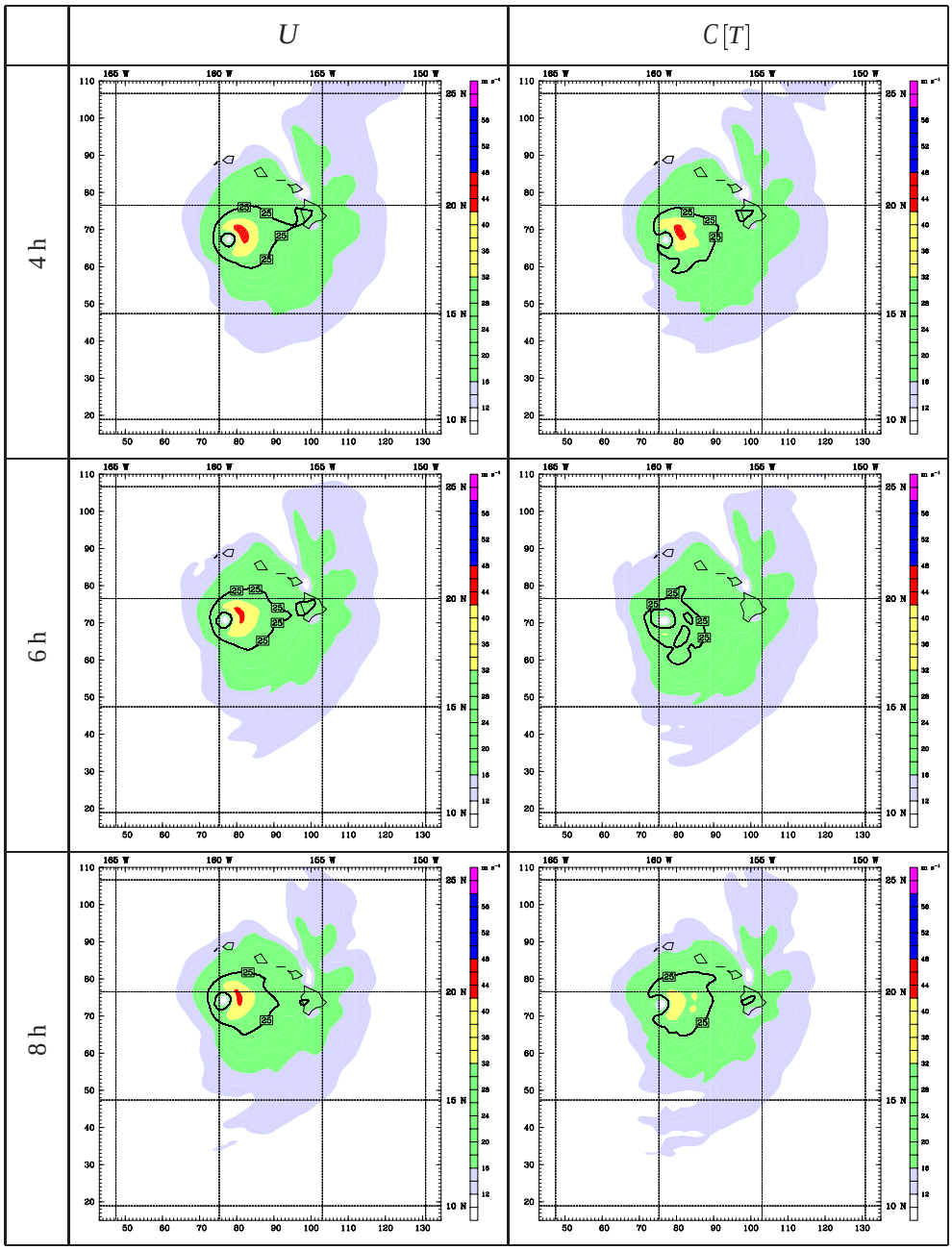

Fig. 6: Perturbations for experiments with different control vectors. Wind at 950 hPa is plotted for experiment $C[V]$, vertical velocity at 650 hPa for $C[w]$, specific humidity at 650 hPa for $C[q]$, and perturbation pressure at 950 hPa for $C[p']$. Wind barbs are in kts. Wind speed in $\mathrm{m\,s^{-1}}$, vertical velocity in $10^{-2}\,\mathrm{m\,s^{-1}}$, specific humidity in $10^{-3}\,\mathrm{kg/kg}$ and perturbation pressure in hPa are color coded.

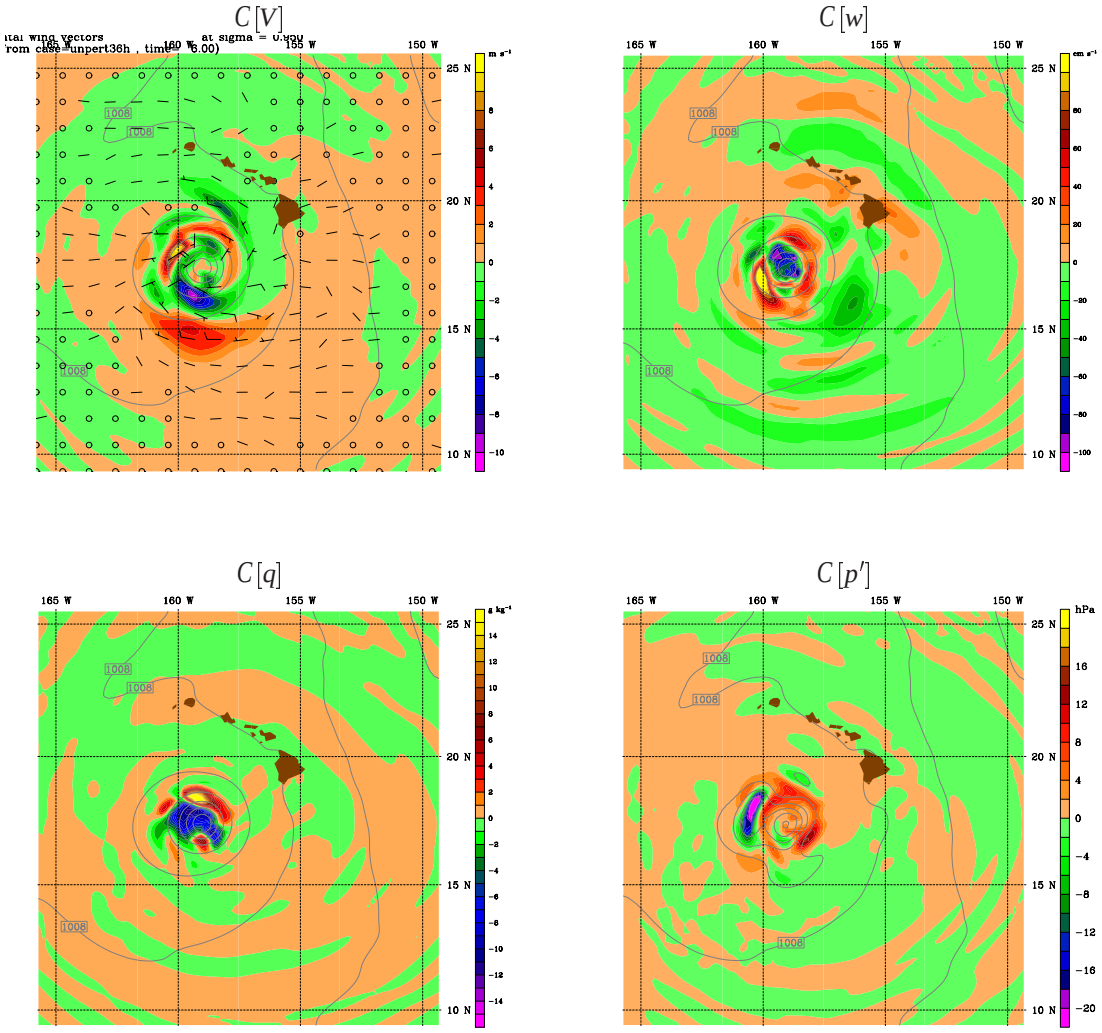

Fig. 7: Structure of the initial perturbation for experiment $L\,[T_a]$. As in Fig. 4, horizontal slices of δT are shown at 950, 650, and 350 hPa. Temperature in degrees C is color coded.

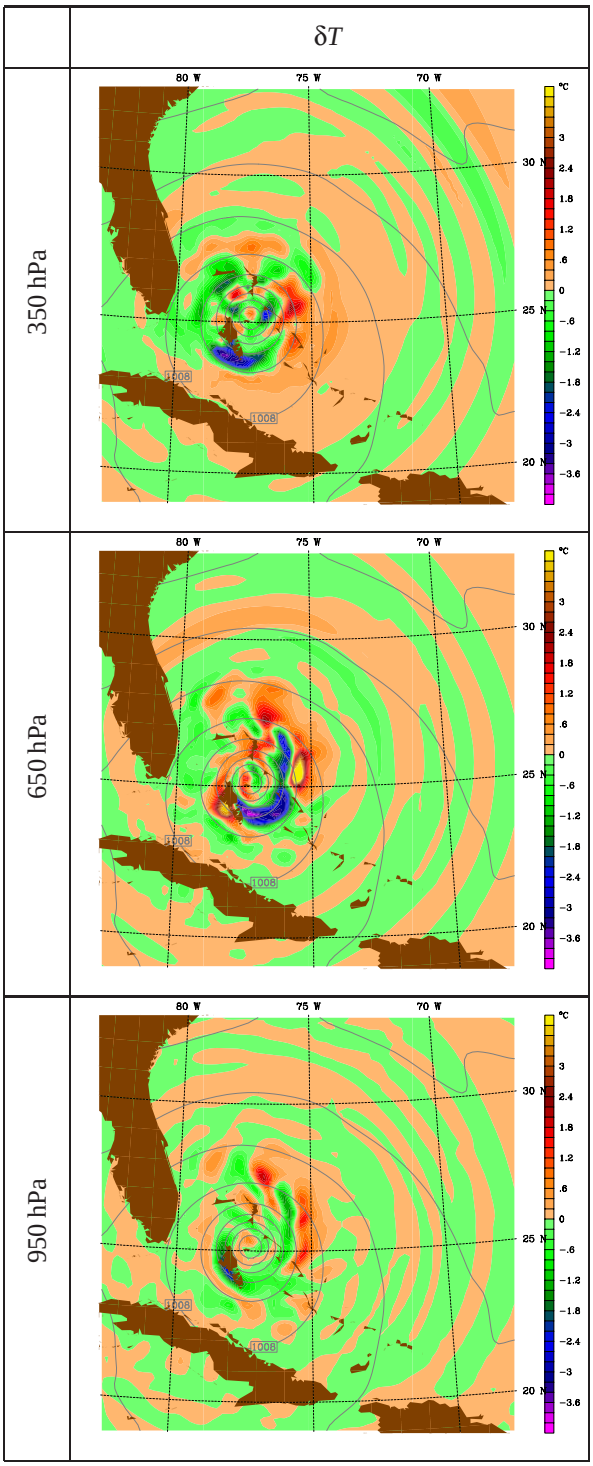

Fig. 8: Evolution of the perturbation for experiment $L\,[T_a]$. Horizontal slices of δT and δV are shown at 350 and 950 hPa respectively, each at 2, 4, 6, and 8 h. Temperature in degrees C and wind speed in m s $^{-1}$ are color coded. A full wind barb represents 5 m s^{-1}.

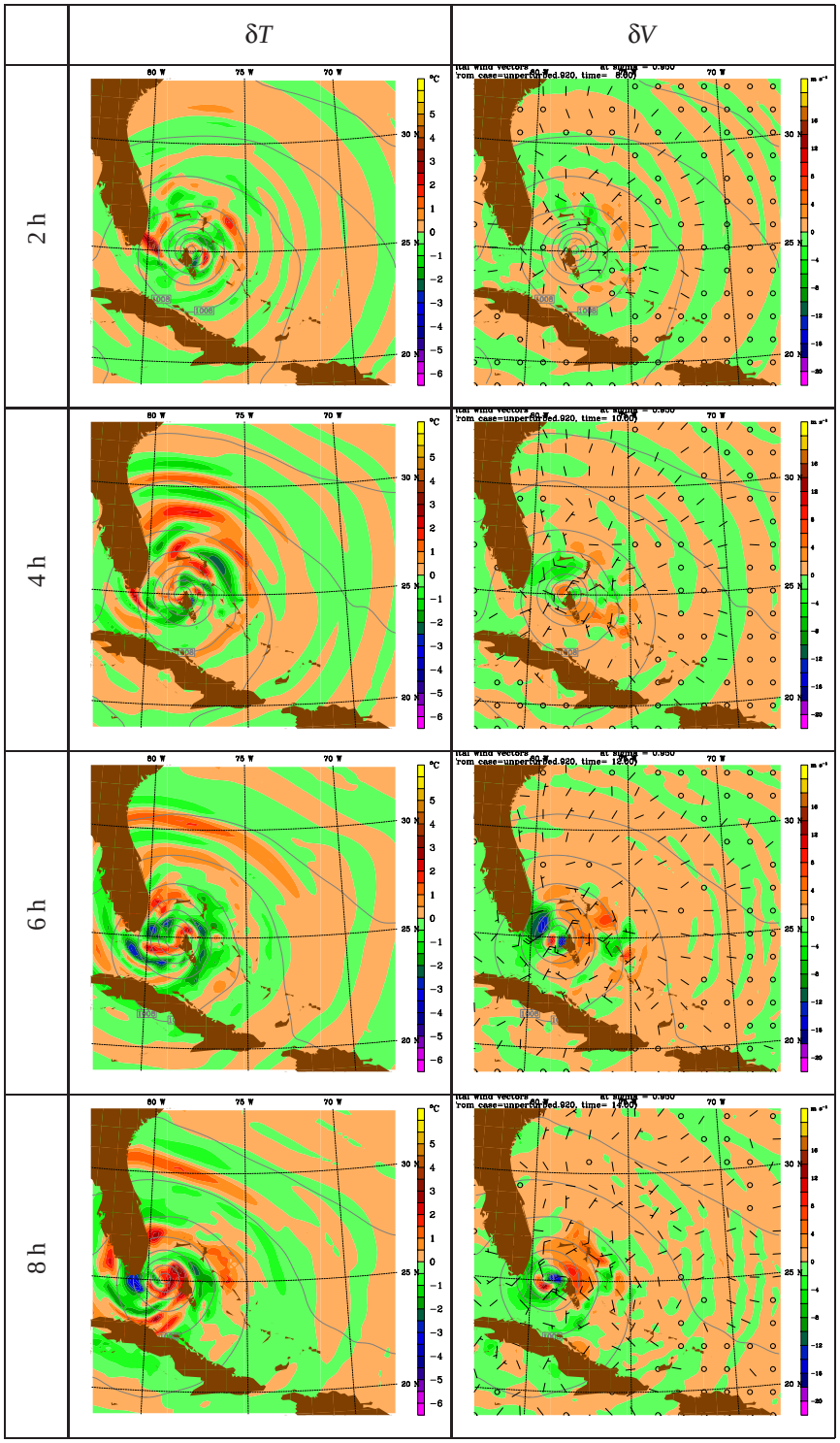

Fig. 9: Evolution of the surface wind field for the unperturbed simulation U_a and for experiment $L[T_a]$. As in Fig. 5: Wind speed is color coded according to the Saffir-Simpson scale and the damaging wind contour $25\ \mathrm{m\ s^{-1}}$ is plotted at 4, 6, and 8 h.